



# Inhibitive Influence of Cumin (*Cuminum Cyminum*) Seed Extract on the Dissolution of Al in 2 M HCl Acid Medium

A. S. Fouda<sup>1</sup> · S. M. Rashwan<sup>2</sup> · M. M. Kamel<sup>2</sup> · E. Abdel Haleem<sup>3</sup>

Received: 12 April 2020 / Revised: 26 December 2020 / Accepted: 20 January 2021 / Published online: 24 February 2021  
© The Author(s), under exclusive licence to Springer Nature Switzerland AG part of Springer Nature 2021

## Abstract

The inhibition influence of Al dissolution by Cumin (*Cuminum Cyminum* extract, CCE) in 2 M HCl has been examined by electrochemical investigations like Tafel polarization (TP), electrochemical frequency modulation (EFM), electrochemical impedance spectroscopy (EIS) and chemical measurements as gasometrical and gravimetric methods at varied temperatures. Langmuir adsorption isotherm was utilized to demonstrate the adsorption procedure relying on estimations of adsorption constant ( $K_{ads}$ ). Maximum value of inhibiting proficiency is 93.1% at 25 °C and 300 ppm of CCE concentration. Surface examinations such as XPS, AFM, and FTIR were applied and confirmed the formation of defensive layer on the Al outer surface. FTIR outcomes illustrated the existence of varied functional groups that make coordination interactions with  $Al^{3+}$ . XPS examination demonstrated the interference among the investigated metal and the molecules exist in CCE. The obtained outcomes demonstrated that CCE can be utilized as beneficial inhibitor for Al in 2 M HCl. All results from the utilized techniques are in consistent values.

**Keywords** Cumin extract (CCE) · TP · FTIR · AFM · XPS

## 1 Introduction

Al metal is utilized in numerous purposes in enterprises (aviation, housekeeping, electronic gadgets, and nourishment industry) because of its low value, high electrical limit, and its high vitality thickness [1, 2]. Despite the fact that Al can frame a stable dainty oxide film which shields it from the corrosion wonder, it experiences corrosion [3–5] while being in contact with corrosive media, for example, hydrochloric corrosive. Dissolution control can be accomplished by numerous techniques; in any case, the utilization of corrosion inhibitors is really the most functional strategy utilized in enterprises and scholarly investigations. A review of the writing illustrates [6–8] that the vast majority of the notable ecofriendly corrosion inhibitors are natural mixes containing

nitrogen, oxygen, sulfur, and additionally  $\pi$  bonds in their sub-atomic structure. A few heterocyclic N, S, or O-containing natural mixes [9–12] have been utilized to impede Al from hydrochloric corrosive dissolution. Restricted corrosion can be dodged by the activity of adsorption inhibitors, which impede the adsorption of forceful anions or by the arrangement of a progressively safe oxide film on the metal surface. Considering the wide range of natural mixes accessible as corrosion inhibitors, there is expanding worry about the harmfulness of most corrosion inhibitors since they are dangerous to living life form and might be poison the earth [13]. These have advanced looks for green corrosion inhibitors. Green corrosion inhibitors are biodegradable and don't contain overwhelming metals or other lethal mixes. Varied plant extracts have been checked as beneficial retardants in destructive mediums [14–26].

The obtained measurements illustrate the inhibitive influence of CCE for Al in M HCl as destructive medium which is on the basis that CCE is estimated as a practical origin, biodegradable, cheap, do not contain heavy metals or other toxic substances, and availability inhibitor. Hydrochloric corrosive is picked as a destructive mechanism for Al since it is broadly utilized in the industrial applications. The study is aimed at establishing the corrosion inhibitive potential and

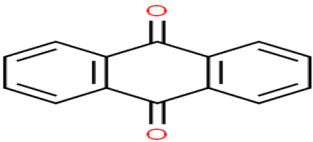
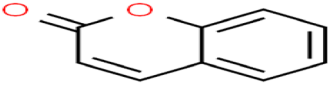
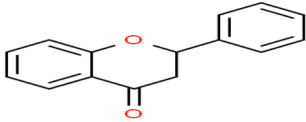
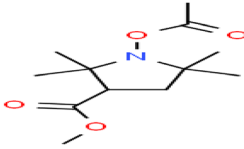
✉ A. S. Fouda  
asfouda@hotmail.com

<sup>1</sup> Department of Chemistry, Faculty of Science, Mansoura University, Mansoura 35516, Egypt

<sup>2</sup> Department of Chemistry, Faculty of Science, Suez Canal University, Ismailia, Egypt

<sup>3</sup> Department of Basic Science, Higher Institute of Engineering and Technology in El-Arish, Arish, Egypt

**Table 1** The names, structures, molecular formulas and molecular weights of the main extract constituents

Name	Structure	Molecular formula
Anthraquinone	 9,10-Anthraquinone	$C_{14}H_8O$
Coumarin	 2H-Chromen-2-one	$C_9H_6O_2$
Flavanone	 4H-1-Benzopyran-4-one, 2,3-dihydro-2-phenyl	$C_{15}H_{12}O_2$
Saponin	 1-Acetoxy-3-methoxycarbonyl-2,2,5,5-tetramethylpyrrolidine	$C_{12}H_{21}NO_4$

mechanism of corrosion inhibition of Al in acid medium by Cumin (*Cuminum Cyminum* extract).

## 2 Materials and Techniques

### 2.1 Solutions and Materials

#### 2.1.1 Al Composition

Al pieces studied in this research were cut from Al with purity of 99.98%. The pieces have volume  $2 \times 2 \times 0.5 \text{ cm}^3$ .

#### 2.1.2 Solutions

The destructive medium (2 M HCl) was got from a stock acid by diluting with bi-distilled  $H_2O$  from the concentrated HCl medium (34%) and its concentration was checked using standard  $Na_2CO_3$  solution.

### 2.1.3 Chemical Composition of CCE Extract

CCE extract consists of several organic compounds (anthraquinone, coumarin, flavanone, steroid hydroperoxide, and tannin) (Table 1) [27, 28].

### 2.1.4 CCE Solution

CCE extract had been gotten from the powder of dried CCE seeds then put in methyl alcohol for 7 days. The fluid medium used to be separated utilizing refinery paper to get rid of methyl alcohol from the Cichorium Intybus liquid and put till lack. A 1000 ml of the extract has prepared from dissolving one gram from the residual in 3 ml of dimethyl sulfoxide (DMSO) and then completed to one liter utilizing  $C_2H_5OH$  (1000 ppm) finally set in refrigerator in tightly closed flasks. The various concentrations of the extract (50–300 ppm) were determined by dilution with bidistilled water.

## 2.2 Utilized Measurements

### 2.2.1 Chemical Calculations

**2.2.1.1 Mass Loss Tests** This trial was applied using seven indistinguishable Al pieces with measurements of (2×2×0.5) cm, which were consummately scratched with varied emery papers. Rinsing and purifying of the samples were applied by Acetone and bi-refined water. The Al samples were dipped in mediums of 100 ml of 2 M HCl in the absence and presence of varied concentration of CCE extract [29–31]. Every 30 min, the samples were got out, rinsed, dried, and weighed at varied temperatures (25–45 °). Surface coverage ( $\theta$ ) and (IE %) can be computed utilizing the accompanying Eq. (1):

$$\%IE = \theta \times 100 = [(W^o - W)/W^o] \times 100 \quad (1)$$

where  $W^o$  and  $W$  are the estimations of the mass loss in the absence and presence of CCE, separately. The calculations of  $\theta$  and % IE were measured at varied amounts of CCE in 2 M HCl.

**2.2.1.2 Hydrogen Emission Tests** The H<sub>2</sub> development is a profitable strategy to calculate the measure of H<sub>2</sub> generating during this operation. The container is joined by a malleable part to a burette. Firstly, the volume of air was observed. At last, Al sheets were put in the destructive solution and the flask was tightly closed. The evaluated H<sub>2</sub> gas was measured by the diminishing of the medium plane in the phial at definite times.

### 2.2.2 Electrochemical Techniques

Electrochemical estimations were finished using the cell of (a) working anode comprises of Al bind with Cu-wire to connect power and settled into a glass container of appropriate measurement to reach territory of Al terminal 1 cm<sup>2</sup>. The working anode is scratched as clarified previously. (b) Saturated calomel cathode (SCE) is the reference anode. Every single potential worth was enlisted versus SCE. (c) Platinum foil (1 cm<sup>2</sup>) is the assistant cathode. In all experiments, The Al electrode could reach a stable open potential (30 min) value,  $E_{\text{corr}}$ . The electrochemical estimations were performed using Potentiostat/Galvanostat/Zra analyzer (Gamry- PCI4G750 USA).

**2.2.2.1 Tafel Polarization Test** Tafel polarization measurements were performed by utilizing a potential extent (−1300 mV to −300 mV) to get the current densities ( $i_{\text{corr}}$ ). The polarization curves were recorded at a constant sweep rate of 1 mV/s. Estimations of corrosion current densities ( $i_{\text{corr}}$ ) and the potential ( $E_{\text{corr}}$ ) were achieved by extrapolat-

ing of both Tafel slopes. IE % and  $\theta$  from Tafel polarization were computed using Eq. 2:

$$\%IE = \theta \times 100 = [(i_{\text{corr}} - i_{\text{corr(inh)}})/i_{\text{corr}}] \times 100 \quad (2)$$

where  $i_{\text{corr(inh)}}$  and  $i_{\text{corr}}$  are the corrosion current density estimations in the existence and nonexistence of CCE, respectively.

### 2.2.2.2 Electrochemical Frequency Modulation (EFM) Tests

EFM is nondestructive corrosion estimation system which can provide estimations of the current without previously results on Tafel parameters. Like EIS, it is a little sign procedure. Not like EIS, two sign waves at varied frequencies (2 and 5 Hz), the base frequency was 0.1 Hz and 10 mV potential distance signals. The bigger tops were utilized to compute the corrosion current ( $i_{\text{corr}}$ ), the Tafel constants ( $\beta_c$  and  $\beta_a$ ), and the causality factors CF-2& CF-3 [32, 33]. All the trials were achieved at 25 ± 1 °C

### 2.2.2.3 Electrochemical Impedance Spectroscopy (EIS) Tests

The impedance trial was done using the frequency range from 100 kHz to 0.1 Hz with 10 mV peak-to-peak signal amplitude perturbation at open-circuit potential (OCP). The major parameters got from the estimation of the Nyquist chart are the polarization resistance  $R_p$  and the capacity of double-layer  $C_{dl}$  which were illustrated [34]:

$$C_{dl} = 1 / (2 \pi f_{\text{max}} R_p) \quad (3)$$

where  $f_{\text{max}}$  is the angular frequency. All measurements got from the impedance trial are computed Eq. (4):

$$\%IE = [1 - (R_p^o / R_p)] \times 100 \quad (4)$$

where  $R_p$  and  $R_p^o$  are the polarization resistance in the existence and absence of CCE extract, respectively.

### 2.2.3 Surface Examination

**2.2.3.1 Fourier Transform Infrared (FTIR) Tests** FTIR spectrum is checked in a Perkin—Elmer 1600 spectrophotometer. The defensive layer was accurately separated and mixed with KBr made in to grains, and FTIR spectrum was resulted.

### 2.2.3.2 X-Ray Photoelectron Spectroscopy (XPS) Tests

XPS check is a quantitative procedure for standardizing the elemental composition of the surface of a material and indicates the binding energies of reacted elements.

### 2.2.3.3 Atomic Force Microscopy (AFM) Analysis

The preferable indication of AFM is the coarseness of the outer surface of Al pieces. AFM examination was checked utilizing

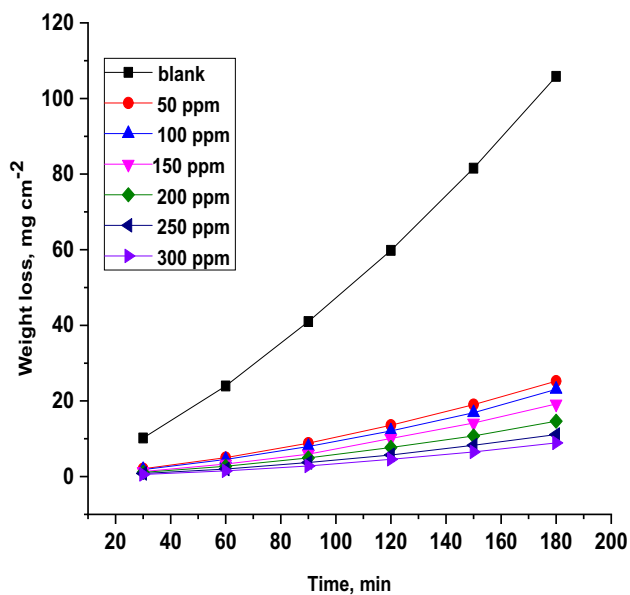


**Fig. 1** Mass loss-time graphs for the corrosion of Al in 2M HCl without and with varied amounts of CCE at 25 °C

**Table 2** Corrosion rate ( $k_{corr}$ ) and inhibition efficiency (%IE) results got from mass loss process for Al in 2 M HCl medium at varied concentrations of CCE at 25 °C

Conc., ppm	$k_{corr}$ mg cm <sup>-2</sup> min <sup>-1</sup>	$\theta$	%IE
Blank	0.455	–	–
50	0.098	0.785	78.5
100	0.088	0.806	80.6
150	0.066	0.855	85.5
200	0.055	0.880	88.0
250	0.041	0.909	90.9
300	0.031	0.931	93.1

Nano Surf Easy sweep 2 Flex AFM procedure (Nanotechnology Center, Mansoura University).

### 3 Results and Discussion

#### 3.1 Mass Loss Calculations

The mass loss of Al in 2 M HCl without and in the existence of varied concentrations (50–300 ppm) of CCE were illustrated. Figure 1 indicates the time mass losses graphs without and with of varied concentrations of CCE at 25°. The mass loss minimized with rising CCE concentration. The obtained calculations about the values of % IE, corrosion rate ( $k_{corr}$ ) and the surface coverage ( $\theta$ ) for Al in 2 M HCl and within varied amounts of CCE at several temperatures are listed in Table 2.

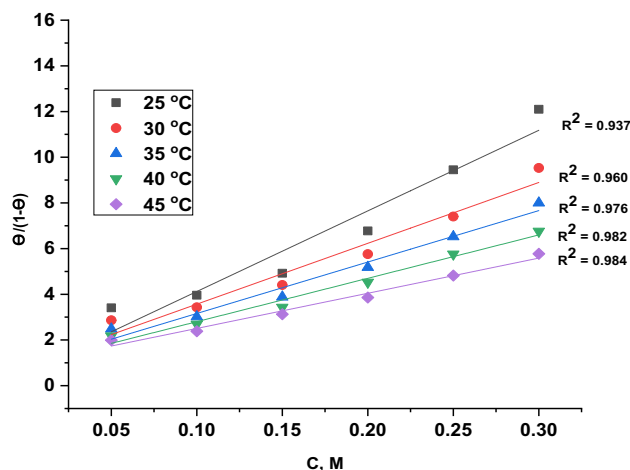


**Fig. 2** Curves of corrosion results for Al in 2 M HCl in the existence of varied concentrations of CCE to the Langmuir isotherm at several temperatures

**Table 3** Thermodynamic parameters for the adsorption of CCE extract on Al surface in 2 M HCl at varied temperatures

Temperature, °C	$-\Delta G^{\circ}_{ads}$ , kJ mol <sup>-1</sup>	$-\Delta H^{\circ}_{ads}$ , kJ mol <sup>-1</sup>	$-\Delta S^{\circ}_{ads}$ , J mol <sup>-1</sup> K <sup>-1</sup>
25	18.8	31.5	42.6
30	18.4		43.2
35	18.3		42.9
40	18.1		42.8
45	17.9		42.8

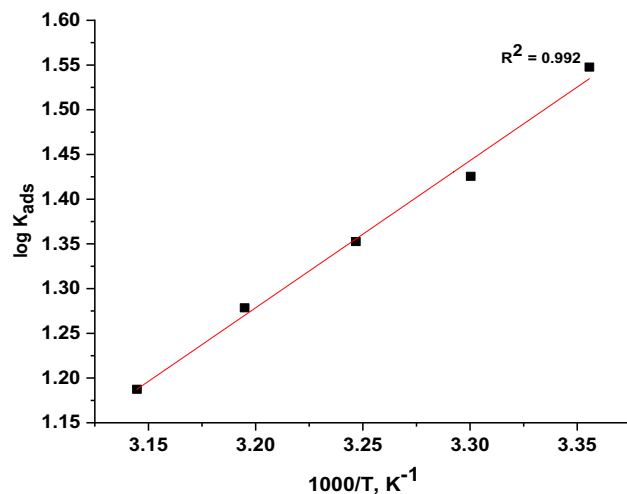


**Fig. 3** Graph of (Log  $K_{ads}$ ) against (1/T) for the corrosion of Al in 2 M HCl in the existence of CCE

### 3.1.1 Adsorption Procedure

For realization, the mode of corrosion inhibiting influence and the adsorption attitude of the CCE adsorbents on the surface ought to be checked. The adsorption mode is reliant on factors, for instance, the structure of the inhibitor and the characteristics of the ionized metal. There are varied numerical relations formed to illustrate nonperfect influences. The familiar isotherms utilized are Frumkin, De Boer, Langmuir, Temkin, Flory–Huggins, and Bockris-Swinkless [35–39]. The calculations of  $(\theta)$  comparing to varied doses of CCE at 25–45 °C have been checked to choose the perfect isotherm procedure. The adsorption of CCE particles is ascribed to the Langmuir adsorption by plotting the relation  $\theta/1 - \theta$  vs.  $C$  (Fig. 2) [40]. The slope of these lines is  $K_{ads}$ , as follows:

$$\left(\frac{\theta}{1 - \theta}\right) = K_{ads}C \tag{5}$$

where  $C$  is the concentration of CCE in the corrosive mediums,  $\theta$  is the surface coverage, and  $K_{ads}$  is the adsorption constant. Lines are got from graphing of  $\text{Log } K_{ads}$  vs.  $1/T$  with slope is  $\Delta H^{\circ}_{ads}$  as checked in Fig. 3. All estimations were resolved. The major factors are the free energy ( $\Delta G^{\circ}_{ads}$ ), the heat of enthalpy ( $\Delta H^{\circ}_{ads}$ ), and the entropy ( $\Delta S^{\circ}_{ads}$ ). The amounts can be computed by varied systems relying on the values of  $K_{ads}$  at several temperatures [41]. The  $\Delta G^{\circ}_{ads}$  can be computed from Eq. (6):

$$K_{ads} = (1/55.5) \exp \left(-\Delta G^{\circ}_{ads}/RT\right) \tag{6}$$

where 55.5 is the concentration of  $H_2O$  in  $\text{mol l}^{-1}$ ,  $R$  is the universal gas constant, and  $T$  is the temperature. ( $\Delta H^{\circ}_{ads}$ ), ( $\Delta S^{\circ}_{ads}$ ) can be demonstrated from Eqs. (7 and 8):

$$\text{Log } K_{ads} = (\Delta H^{\circ}_{ads}/2.303RT) + \text{constant} \tag{7}$$

$$\Delta G^{\circ}_{ads} = \Delta H^{\circ}_{ads} - T\Delta S^{\circ}_{ads} \tag{8}$$

Table 3 demonstrates all the calculated parameters for the extract on Al surface, and illustrates that the sign of  $\Delta G^{\circ}_{ads}$  was negative that illustrates that the adsorption of CCE is spontaneous procedure. The estimations of  $\Delta G^{\circ}_{ads}$  of  $40 \text{ kJ mol}^{-1}$  and more referred to charge moving from the inhibitor molecules to metal outer surface (chemisorption); those of  $20 \text{ kJ mol}^{-1}$  and smaller assumed the electrostatic attraction among the inhibited charged surface and charged molecules of the extract (physisorption) [42, 43].

The resulted estimations of  $\Delta G^{\circ}_{ads}$  are  $-20 \text{ kJ mol}^{-1}$  and lower that ascribed to the electrostatic attraction among the charged extract molecules and the charged metal (physical adsorption).  $\Delta G^{\circ}_{ads}$  values improved (more positive) with rising temperature which indicates that the adsorption mode is an exothermic procedure. The negative sign of  $\Delta H^{\circ}_{ads}$  illustrates that the adsorption mode of the extract molecules is an exothermic method. An exothermic process is ascribed to either physisorption or chemisorption while endothermic mode is credited to chemisorption [44]. Enthalpy measures up to  $41.9 \text{ kJ mol}^{-1}$  are ascribed to physisorption but those equal to  $100 \text{ kJ mol}^{-1}$  or more are referred to chemisorption. The results got of  $\Delta H^{\circ}_{ads}$  of CCE extract in 2 M HCl are negative exhibiting that it may be physisorbed. The  $\Delta S^{\circ}_{ads}$

**Fig. 4** Arrhenius graphs for Al corrosion rates ( $k_{corr}$ ) after 90 min of dipping in 2 M HCl in the absence and presence of varied concentrations of CCE extract

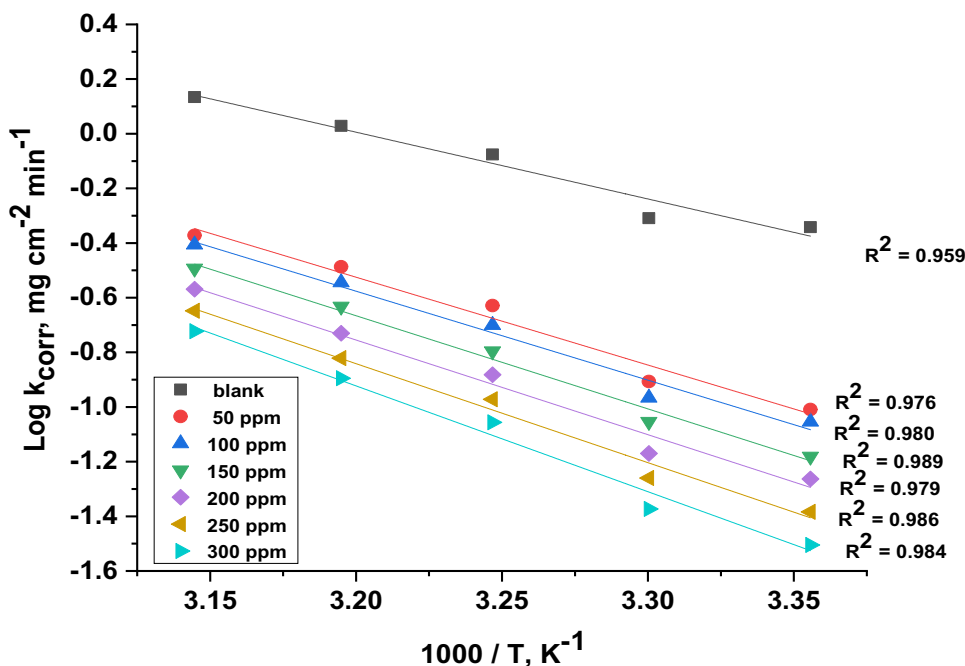


**Table 4** Activation measurements for Al corrosion without and with varied amounts of CCE in 2 M HCl

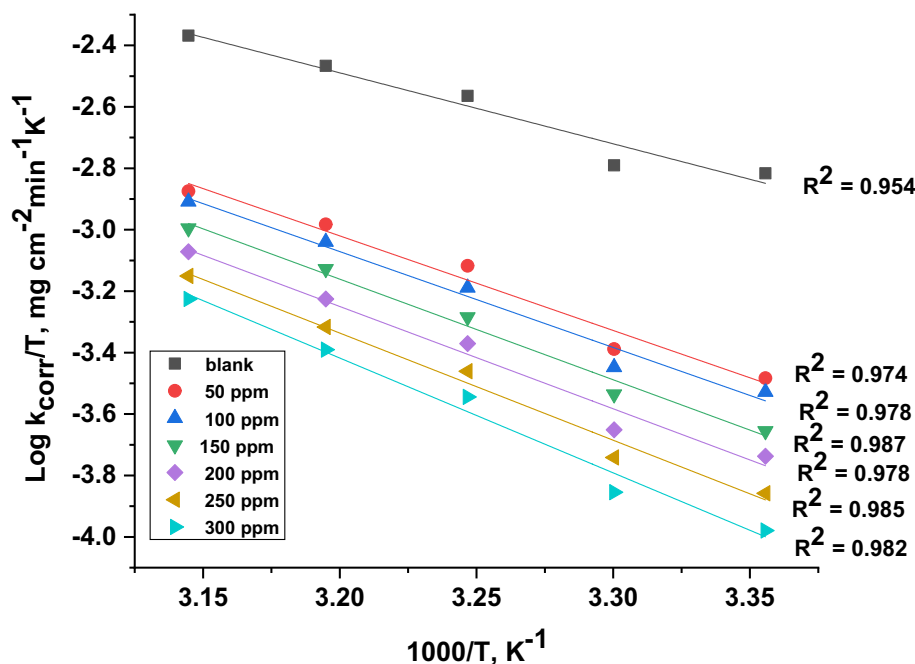
Conc., ppm	Activation calculations		
	$E_a^*$ , kJ mol <sup>-1</sup>	$\Delta H^*$ , kJ mol <sup>-1</sup>	$-\Delta S^*$ , J mol <sup>-1</sup> K <sup>-1</sup>
Blank	46.6	44.3	103.4
50	61.5	58.8	66.7
100	62.3	59.7	65.1
150	65.3	62.6	57.4
200	66.3	63.7	55.8
250	69.4	66.6	47.7
300	74.1	71.4	34.0

**Table 5** IE% and ( $k_{corr}$ ) from HE for the corrosion of Al in 2 M HCl without and with varied concentrations of CCE extract at 25 °C

Conc., ppm	$k_{corr} \times 10^{-3}$ , ml/min	%IE
Blank	1200	–
50	213	82.3
100	163	86.4
150	144	88.0
200	126	89.5
250	109.5	90.9
300	100	91.7

values are negative that is specified to exothermic adsorption procedure and illustrated that the extract molecules moving clearly in the electrolyte and were adsorbed in an orderly mode onto the Al surface.

**Fig. 5** Transition state for Al corrosion rates ( $k_{corr}$ ) in 2 M HCl with and without varied doses of CCE extract



### 3.1.2 Temperature Impact and Activation Factors of Inhibition Process

The impact of temperature on the corrosion rate of Al in 2 M HCl without and in the with of the examined extract was illustrated in temperatures limit from 25 to 45 °C. The inhibitive protection lowered with rising temperature and the rate of corrosion rises. The lowering in the inhibition performance with temperature is ascribed to desorption of CCE particles from the tested surface. Energy of activation was obtained from the next Arrhenius-type equation:

$$k_{corr} = A \exp (E_a^*/RT) \tag{9}$$

where  $k_{corr}$  is the corrosion rate,  $E_a^*$  is the activation energy,  $R$  is the universal gas constant,  $T$  is the temperature, and  $A$  is the Arrhenius parameter. Calculation of  $E_a^*$  of corrosion for Al in 2 M HCl without and with varied amounts of CCE was obtained from the graphing of  $\log (k_{corr})$  versus  $1/T$  and is represented in Fig. 4. The transition state relationship is obtained in Eq. (10):

$$k_{corr} = (RT/Nh) \exp (\Delta S^*/R) \exp (-\Delta H^*/RT) \tag{10}$$

where  $h$  is the Planck's steady,  $N$  is the Avogadro's number,  $\Delta S^*$  is the activated entropy, and  $\Delta H^*$  is the activated enthalpy. Figure 5 illustrates ( $\log k_{corr}/T$ ) versus ( $1/T$ ). Straight lines are got with slopes proportional to ( $\Delta H^*/2.303R$ ), and their calculations are listed in Table 4. The elevation in  $E_a^*$  in the existence of CCE than in its absence illustrates that the extract is physisorbed on the Al metal surface [45]. Table 5 explains that  $E_a^*$  rises with

**Fig. 6** Amounts of emitted H<sub>2</sub> gas vs. time for corrosion of Al in 2 M HCl with and without varied concentrations of CCE extract at 25 °C

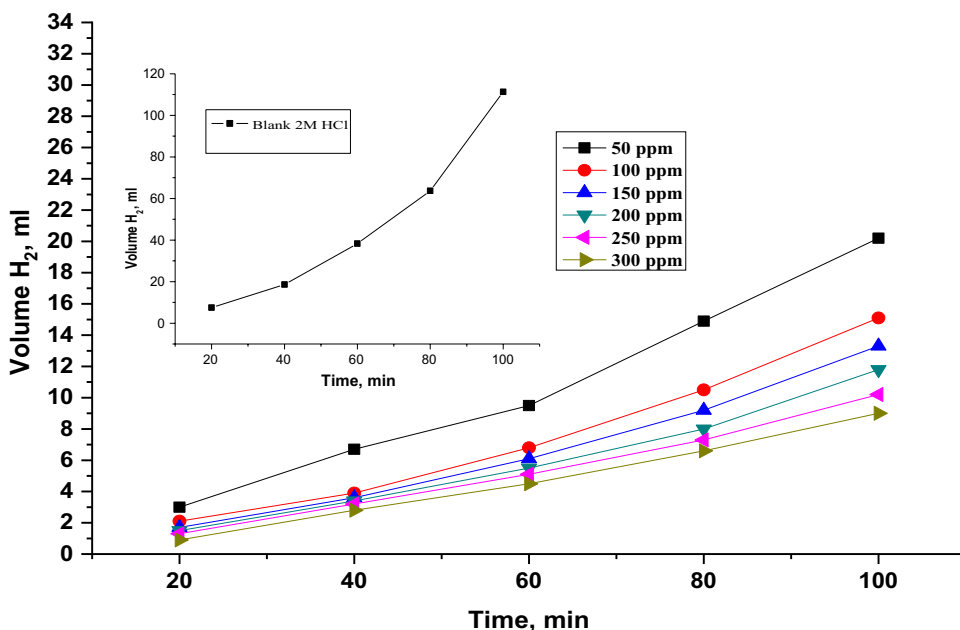


**Table 6** Results from Tafel plots of Al in 2 M HCl having varied concentrations of CCE extract at 25 °C

Conc., ppm	$-E_{corr}$ , mV (vs SCE)	$i_{corr}$ , mA cm <sup>-2</sup>	$\beta_a$ , mV dec <sup>-1</sup>	$-\beta_c$ , mV dec <sup>-1</sup>	C.R., mpy	$\theta$	% IE
0	774.0	847.0	76.5	52.3	363.9	–	–
50	753.3	245.7	19.8	31.6	94.6	0.709	70.9
100	781.0	208.0	17.2	20.5	89.1	0.754	75.4
150	775.1	139.2	13.5	23.8	59.8	0.836	83.6
200	782.2	116.4	23.4	35.6	49.9	0.863	86.3
250	788.5	27.5	22.1	25.3	11.8	0.968	96.8
300	797.7	15.6	12.9	19.6	6.7	0.982	98.2

improving CCE concentrations, which recommended the adsorption of the tested extract on the Al surface. The positive indications of  $\Delta H^*$  illustrated the endothermic mode of the Al corrosion procedure. The negative  $\Delta S^*$  demonstrates that in the rate governing stage, the association of unstable coordinated molecules is higher than the dissociation [46, 47].

### 3.2 Gasometrical Tests

The evolved H<sub>2</sub> gas coming about due to the corrosion procedure can be illustrated. Outcomes got by the H<sub>2</sub> development in Fig. 6 are organizing with varied measurements like mass difference and electrochemical procedures. The H<sub>2</sub> amount is relied on time of response as the following Eq. (11):

$$V_{ml} = k_{corr} \cdot t \tag{11}$$

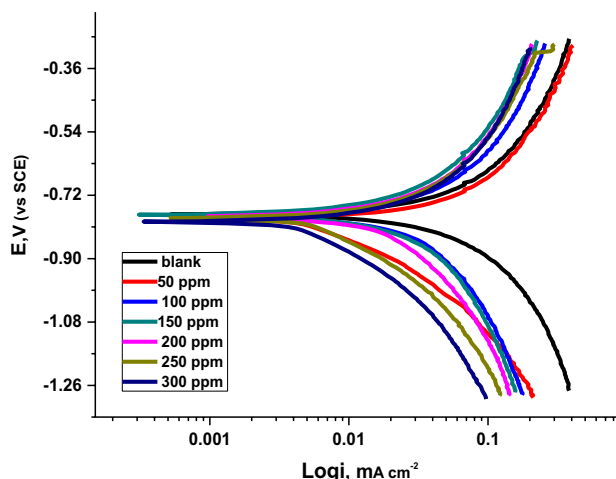


**Fig. 7** Tafel polarization graphs for the corrosion of Al in 2 M HCl without and with varied concentrations of CCE extract at 25 °C

$V$  is the volume of the  $H_2$  emitted in ml,  $t$  represents time, and  $k_{\text{corr}}$  is corrosion rate at  $25^\circ\text{C}$  [48].

The  $H_2$  amount was computed every 20 min;  $k_{\text{corr}}$  and % IE were computed by Eq. (12):

$$\%IE = (1 - K/K_0) \times 100 \quad (12)$$

$K$  and  $K_0$  are the  $k_{\text{corr}}$  in existence and nonexistence of varied doses of CCE, by graphing among ( $V_{\text{ml}}$  vs.  $t$ ) and slope is  $k_{\text{corr}}$ .

### 3.3 Tafel Polarization (TP) Tests

Tafel polarization graphs for Al in 2 M HCl arrangement in the nonappearance and nearness of changed amounts of CCE at  $25^\circ\text{C}$  are appeared in Fig. 7 and the polarization factors, for example,  $E_{\text{corr}}$ ,  $i_{\text{corr}}$ ; anodic and cathodic Tafel slopes ( $\beta_a$ ,  $\beta_c$ ) are listed in Table 6. Anodic and cathodic Tafel slants were lightly changed on expanding CCE extract amounts. This implies there is no difference in the instrument of the inhibition in attendance and nonattendance of CCE extract and this inhibitor influences both cathodic and anodic responses [49]; for example, it is mixed kind inhibitor with little varieties in the  $E_{\text{corr}}$  estimations of the blank examples. The level of surface coverage ( $\theta$ ) and inhibitive proficiency (% IE) were computed.

### 3.4 Electrochemical Frequency Modulation (EFM) Tests

EFM is a nondestructive dissolution estimation system that can immediately compute the corrosion current without earlier information on Tafel slants and with just a little polarizing signal. These favorable indications of EFM method make it a perfect possibility for online corrosion observing [50]. The perfect quality of the EFM is the causality factors which appear as an interior examination on the veracity of EFM estimation. The EFM spectrum of Al in 2 M HCl medium having (50–300 ppm) of CCE at  $25^\circ\text{C}$  is appeared in Fig. 8. The bigger tops were utilized to compute the corrosion current ( $i_{\text{corr}}$ ), the Tafel slopes ( $\beta_c$  and  $\beta_a$ ), and the causality factors (CF-2 and CF-3) [51]. All electrochemical estimations are recorded in Table 7 illustrating that CCE impedes the corrosion of Al in 2 M HCl through adsorption. The causality factors got under various test conditions are around equivalent to the theoretical qualities (2 and 3) demonstrating that the observed information is checked and of perfect quality [52]. The  $IE_{\text{EFM}}$  rises with rising CCE extract amounts and was determined as follows: where  $i_{\text{corr}}^0$  and  $i_{\text{corr}}$  are corrosion current densities in the nonpresence and presence of CCE, separately.

**Table 7** Electrochemical outcomes got from EFM for in the nonexistence and existence of varied amounts of CCE extract at  $25^\circ\text{C}$

Conc., ppm	$i_{\text{corr}}$ , $\mu\text{A cm}^{-2}$	$\beta_a$ , $\text{mV dec}^{-1}$	$-\beta_c$ , $\text{mV dec}^{-1}$	CF-2	CF-3	C.R, mpy	$\theta$	%IE
Blank	831.4	67.4	39.1	1.85	1.68	357.0	–	–
50	282.1	52.2	22.2	2.37	1.94	121.1	0.661	66.1
100	265.3	44.8	21.3	2.67	1.82	113.9	0.681	68.1
150	245.3	35.8	20.5	2.82	2.07	105.3	0.705	70.5
200	239.6	31.2	20.9	2.94	3.12	102.9	0.712	71.2
250	222.8	28.9	18.7	2.46	1.97	95.6	0.732	73.2
300	204.1	24.5	16.0	1.88	3.03	87.6	0.755	75.5

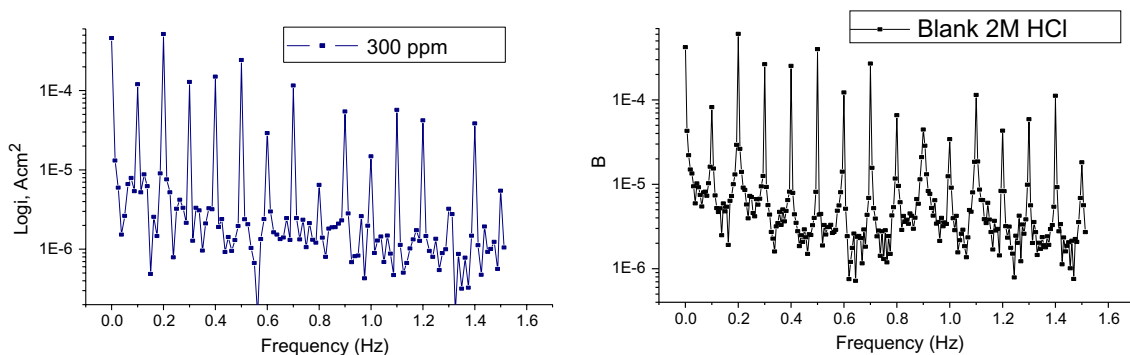


**Fig. 8** EFM spectrum for Al in 2 M HCl in the nonexistence and existence of 300 ppm of CCE at  $25^\circ\text{C}$



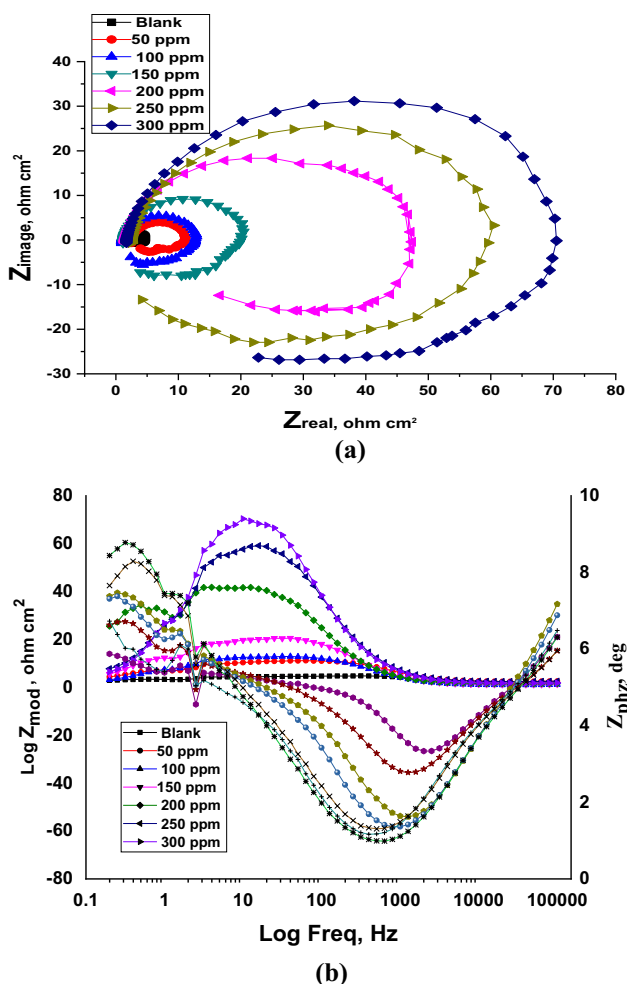


**Fig. 9** Nyquist graphs (a) and Bode graphs (b) for Al in 2 M HCl in the nonattendance and existence of varied amounts of CCE extract at 25 °C

### 3.5 Electrochemical Impedance Spectroscopy (EIS) Tests

The corrosion of Al in 2 M HCl medium with and without various concentrations of CCE was clarified by the EIS methodology at 25 ± 1 °C during 30 min of submersion.

**Table 8** Electrochemical calculations resulted from EIS method for Al in 2 M HCl in the nonattendance and attendance of different amounts of CCE extract at 25 °C

Conc., ppm	$L_s$ , H cm <sup>2</sup>	$R_{ct}$ , Ω cm <sup>2</sup>	$R_L$ , Ω cm <sup>2</sup>	$R_p$ , Ω cm <sup>2</sup>	$C_{dl}$ , μF cm <sup>-2</sup>	$\theta$	%IE
Blank	1.73	4.62	2.11	1.44	75.67	–	–
50	10.35	10.16	12.64	5.62	36.89	0.744	74.4
100	13.91	11.69	16.98	6.94	31.76	0.793	79.3
150	14.15	15.04	17.21	8.02	26.36	0.821	82.1
200	16.55	19.53	20.21	9.94	22.23	0.855	85.5
250	19.91	22.25	24.32	11.63	18.83	0.876	87.6
300	23.20	25.81	28.345	13.51	13.56	0.893	89.3

Fig. 9a, b outlines the Nyquist and Bode diagrams for Al in 2 M HCl with and without the existence of altered concentrations of the examined extract. The way that EIS diagrams have an around semi-round event exhibits that the corrosion of Al in 2 M HCl is controlled by a charge move resistance strategy. A bit of twisting was found in specific systems, and the distortion has been credited to continue scattering [53] because of surface roughness, impurities, divisions, grain boundaries, plan of exposed layers, and Heterogeneity of the uncovered surface. The width of the capacitive loop increases with the expansion of dose and rises of the grade of inhibitive mechanism. Despite the elevated frequency capacitive loop, the semi-loops turned and stretched up to the 4th fourth quadrant, and an artificial-inductive loop at lower frequency extent was observed illustrating that the faradic technique is occurring on the terminal areas. The inductive loop is all around credited to the adsorption of kinds coming about on account of the Al dissolution and the H<sub>2</sub> adsorption [54]. The best equivalent circuit that matches the experimental data of the Nyquist plots is presented in Fig. 10,  $R_s$  (the first intersection of the semicircle with  $Z_{real}$  axis) represents the resistance of the corrosive medium,  $R_{ct}$  (the second intersection of the semicircle with  $Z_{real}$  axis) is the charge transfer resistance,  $L$  is the inductance, which is intimately associated with the inductive loop at low frequencies,  $R_L$  is the inductive resistance, and  $C_{dl}$  is the capacitance of double layer. After the fitting procedure, these electrochemical parameters are recorded in Table 8. Exactly when an inductive circle is accessible, the resistance of polarization ( $R_p$ ) is resolved from Eq. [13]:

$$R_p = (R_{ct} \times R_L) / (R_{ct} + R_L) \tag{13}$$

EIS results from Table 8 demonstrate that the  $R_p$  values rise and the  $C_{dl}$  diminish with the increase of amount of CCE extract. This is due to the replacement of water (H<sub>2</sub>O) molecules adsorbed on metal surface by CCE molecules on the examined metal and decrease the corrosion procedure. The larger  $R_p$  values are ascribed to a more inhibiting mode [55, 56]. The decreasing in the  $C_{dl}$  is due to the increase of

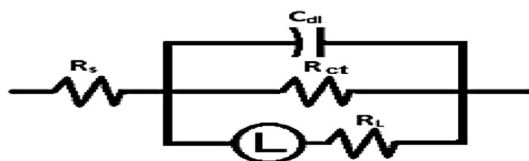


Fig. 10 Electrical equivalent circuit utilized to fit EIS calculations

the dielectric constant or possibly from the increase in the thickness of the electrical double layer [57], indicating that the CCE molecules impede the dissolution by adsorption at the metal/arrangement interface. Also, L and R<sub>L</sub> values increase by increasing the concentration of the extract.

### 3.6 FTIR Examination

FTIR check was carried out for distinguishing of the existing functional groups in organic particles on the Al surface from the extent of 4000 to 400 cm<sup>-1</sup>. Figure 11 demonstrates the IR extent of the pure extract and illustrates that the defensive form was founded on the Al after submersion for 4 h in 2 M HCl utilizing the extract with the ideal dose (300 ppm). In the spectrum of the pure extract in Fig. 11 (Blue curve), the frequency at 3330 cm<sup>-1</sup> is ascribed to the broad (OH), the stretching SP<sub>3</sub>-C-H frequency at 2974 cm<sup>-1</sup>, 2928 cm<sup>-1</sup>, and 2882 cm<sup>-1</sup>, the stretching -C=O frequency at 1653 cm<sup>-1</sup>, the stretching -CH<sub>3</sub> and -CH<sub>2</sub> frequency at 1380 cm<sup>-1</sup> and 1454 cm<sup>-1</sup>, the bending -C-N- frequency shows up at 1047 cm<sup>-1</sup> and the bending =C-H and =CH<sub>2</sub> appears at 880 cm<sup>-1</sup>. FTIR demonstrated a resistance obstruction for

Fig. 11 IR spectrum of pure extract and dissolution products of Al after the mass loss trial having 300 ppm of CCE at 25 °C

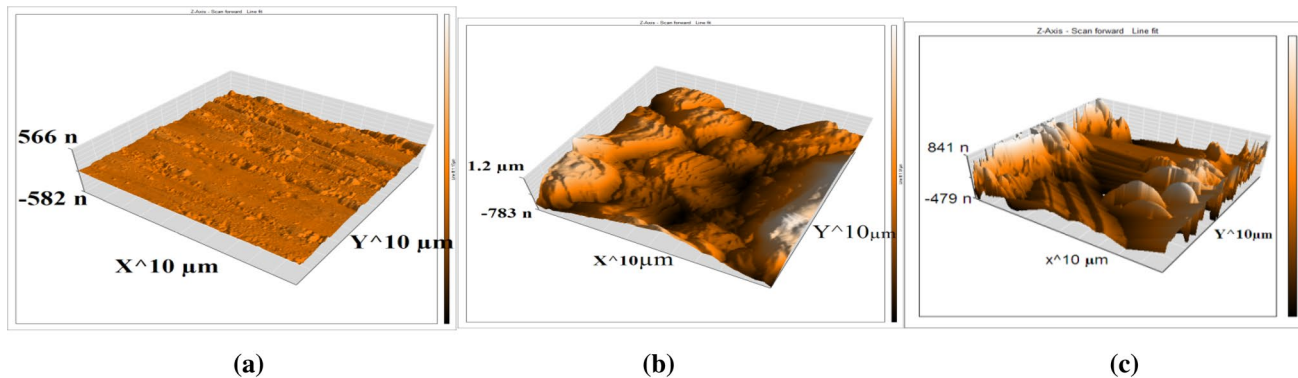
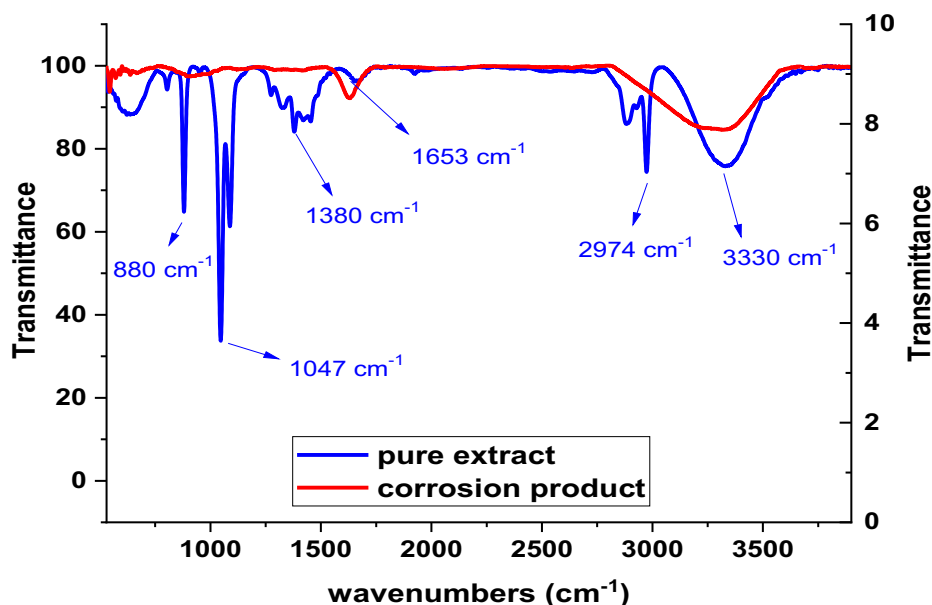


Fig. 12 3D AFM micrographs of the surface of: **a** cleaned Al surface; **b** Al dipped in 2 M HCl; **c** Al dipped in 2 M HCl having *Cichorium intybus* extract (300 ppm)

Al in 2 M HCl containing 300 ppm of the checked extract after submersion for 4hrs [58].

The outcomes illustrated that there were changes and more function group frequencies shifted, and others missed due to interference and coordination with  $Al^{3+}$ . In the inhibited mediums, the corrosion of Al was diminished by the consistence of a defensive form [59, 60].

### 3.7 Atomic Force Microscopy (AFM) Analysis

AFM is a significant trial to check the coarseness of the studied surface at a most maximum resolution in fraction of nanometer [61]. AFM check can provide exact details about the surface morphology of Al that is profitable to corrosion procedure. The 3D of AFM micrographs is appeared in Fig. 12.

The checked surface in 2 M HCl has more coarseness (381.1 nm) than the cleaned Al outer surface (15.6 nm), which illustrates that the checked surface is genuinely corroded in the destructive medium. The estimated coarseness of inhibited Al is minimized (138.11 nm). The observed

softness is because of the forming of a compressed adsorbed layer on the outer surface and then hindering the dissolution of Al [62].

### 3.8 X-ray Photoelectron Spectroscopy (XPS) Analysis

XPS check was utilized to provide exact details into the chemical nature of the interface among the checked inhibitor and the Al outer surface. The XPS spectrum of Al 2p, C 1s, Cl 2p, N 1s, and O 1s got for Al after submersion in 2 M HCl medium in the existence of 300 ppm of (CCE) for 24 h following deconvolution as observed in (Fig. 13). The Al 2p spectrum demonstrated one peak present at a binding energy (BE) of 74.25 eV that ascribed to  $Al_2O_3$  (Fig. 13a) [63]. The spectrum of C 1s (Fig. 13b) is deconvoluted into five tops: the top at 284.37 eV that is referred to (C–C) bond in aromatic rings, the next peak situated at 284.99 eV binding energy which is ascribed to the (C–O–C) aromatic bonds, the third top at 288.25 eV which referred to (C=O), and the tops situated at 289.03 eV and 290.32 eV that correspond

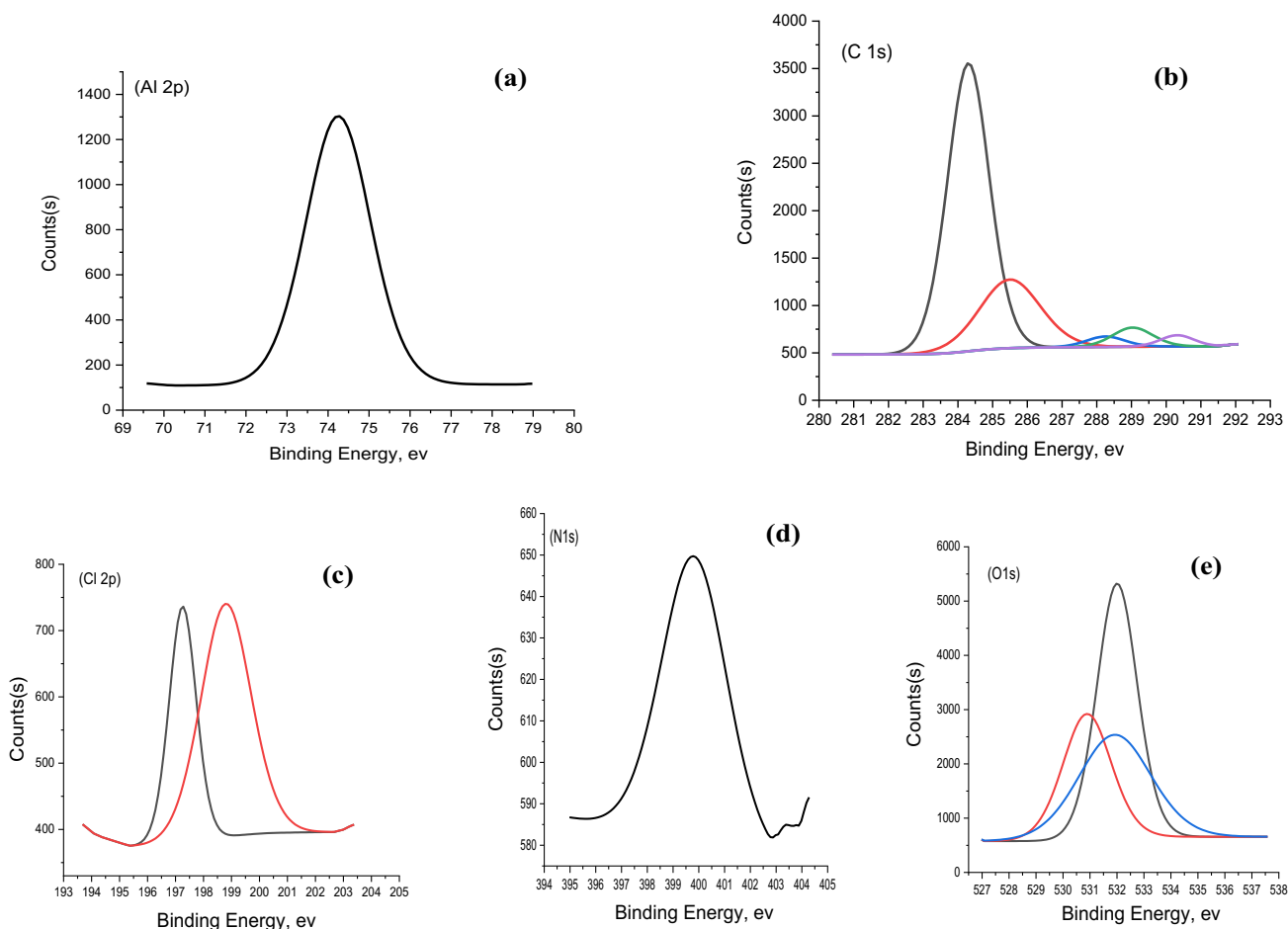


**Fig. 13** XPS micrographs of **a** Al 2p, **b** C 1s, **c** Cl 2p, **d** N 1s, and **e** O 1s for Al in 2 M HCl

to (–COO) [64]. The Cl 2p (Fig. 13c) is deconvoluted into two tops existed at 197.28 eV for Cl 2p<sub>3/2</sub> and 198.49 eV for Cl 2p<sub>1/2</sub> [65]. The spectrum of N 1s is observed as one peak that located at 399.81 eV which referred to N in aromatic rings (Fig. 13d). The spectrum of O1s (Fig. 13e) is deconvoluted into three peaks, The first top at 530.89 can be attributed to Al(OH)<sub>3</sub>, the second one at 531.9 eV that ascribed to C–O bond, and the third top situated at 532.0 eV binding energy that referred to the C–O–C aromatic bonds. Finally, the XPS spectrum indicated the existence of defensive film of CCE extract.

### 3.9 Inhibitive Mechanism

Dissolution occurs by two principle responses: oxidation response and H<sub>2</sub> release. Inhibitive procedure of Al in acidic medium is usually recognized by the adsorption procedure of the molecule onto the Al surface. The organic molecules present in the extract hindered corrosion most likely by diminishing the both responses. There are several variables affecting the inhibiting efficiency of the inhibitor including metal kind, molecular volume, destructive solution, the electronic structure, adsorption positions, substance properties, and process of interference by the supplementary relations: Cl<sup>–</sup> ions are adsorbed on the Al positively charged surface converted it to negative sign, then the protonated molecules of CCE were adsorbed on the negative surface. From our results, the adsorption of these molecules of CCE occurs, decreasing the corrosion reaction. The adsorption is recognized to occur through the anodic sites likely happened through lone  $\pi$ -electrons of aromatic rings in CCE molecules. XPS tests illustrated that the molecules exist in CCE were adsorbed on the Al surface, proving its inhibitive power.

## 4 Conclusions

In this research, the impact of CCE extract as ecofriendly inhibitor on Al corrosion in 2 M HCl acid medium was examined by chemical and electrochemical techniques. The results illustrated that by improvement the amount of CCE has diminished the mass loss, corrosion rate,  $i_{\text{corr}}$ , and  $C_{\text{dl}}$  of Al pieces in 2 M HCl but increasing  $R_{\text{ct}}$ , thereby raising the inhibiting efficiency. The PP curves indicate the extract acts as mixed type inhibitor. The adsorption of the extract molecules on Al surface was physically and followed Langmuir isotherm. Micrographs resulted from all surface examinations showed that the coarseness on the Al surface became lower as the amount of CCE increased, which proofs the impeding of corrosion attacked on Al surface.

## References

- Patel AS, Panchal VA, Mudaliar GV, Shah NK (2013) Impedance spectroscopic study of corrosion inhibition of Al-pure by organic Schiff base in hydrochloric acid. *J Saudi Chem Soc* 17:53–59
- Abdel Gaber AM, Abd El Nabey BA, Sidahmed IM, El Zayady AM, Saadawy M (2006) Kinetics and thermodynamics of Al dissolution in 1.0 M sulphuric acid containing chloride ions. *Mater Chem Phys* 98:291–297
- Berrada S, Elboujdaini M, Ghali E (1992) Comportement électrochimique des alliages Al 2024 ET 7075 dans un milieu salin. *J Appl Electrochem* 22:1065–1071
- Szklarska Smialowska Z (1992) Insight into the pitting corrosion behavior of Al alloys. *Corros Sci* 33:1193–1202
- Ambat R, Dwarakadasa ES (1994) Studies on the influence of chloride ion and pH on the electrochemical behavior of Al alloys 8090. *J Appl Electrochem* 24:911–916
- Yurt A, Ulutas S, Dal H (2006) Electrochemical and theoretical investigation on the corrosion of Al in acidic solution containing some Schiff bases. *Appl Surf Sci* 253:919–925
- Negm NA, Kandile NG, Badr EA, Mohammed MA (2012) Gravimetric and electrochemical evaluation of environmentally friendly nonionic corrosion inhibitors for carbon steel in 1M HCl. *Corros Sci* 65:94–103
- Bommersbach P, Alemany-Dumont C, Millet JP, Normand B (2005) Formation and behavior study of an environment friendly corrosion inhibitor by electrochemical methods. *Electrochim Acta* 51:1076–1108
- Li X, Deng S, Fu H (2011) Inhibition by tetradecylpyridiniumbromide of the corrosion of Al in hydrochloric acid solution. *Corros Sci* 53:1529–1536
- Afak SS, Dura B, Yurt A, Turkoglu GT (2012) Schiff bases as corrosion inhibitor for Al in HCl solution. *Corros Sci* 54:251–259
- Loto RT, Loto CA, Popoola API (2012) Corrosion inhibition of thiourea and thiazole derivatives: a review. *J Mater Environ Sci* 3:885–894
- Fouda AS, Shalabi K, Mohamed NH (2014) Corrosion inhibition of Al in hydrochloric acid solutions using some chalcone derivatives. *Int J Innov Res Sci Eng Technol* 3:9861–9875
- Okon Eddy NI, Ita BN, Dodo SD, Paul E (2012) Inhibitive and adsorption properties of ethanol extract of Hibiscus sabdariffa calyx for the corrosion of mild steel in 0.1 M HCl. *Green Chem Lett Rev* 5:43–49
- Eddy NO, Ibok UJ, Ebenso EE (2010) Adsorption, synergistic inhibitive effect and quantum chemical studies of ampicillin (AMP) and halides for the corrosion of mild steel in H<sub>2</sub>SO<sub>4</sub>. *J Appl Electrochem* 40:445–450
- Fouda AS, Megahed HE, Fouad N, El-bahrawi NM (2016) Corrosion inhibition of carbon steel in 1 M hydrochloric acid solution by aqueous extract of thevetia peruviana. *J Bio Tribo Corros* 2:1–16
- Souza FS, Giacomelli C, Goncalves RS, Spinelli A (2012) Adsorption behavior of caffeine as a green corrosion inhibitor for copper. *Mater Sci Eng* 32:2436–2444
- Abdel Nazeer A, Shalabi K, Fouda AS (2015) Corrosion inhibition of carbon steel by Roselle extract in hydrochloric acid solution: electrochemical and surface study. *Res Chem Intermed* 41:4833–4850
- Njoku DI, Ukaga I, Ikenna OB, Oguzie EE, Oguzie KL, Ibisi N (2016) Natural products for materials protection: corrosion protection of Al in hydrochloric acid by Kola nitida extract. *J Mol Liq* 219:417–424
- Khadraoui A, Khelifa A, Hachama K, Mehdaoui R (2016) Thymus algeriensis extract as a new eco-friendly corrosion inhibitor for 2024 Al alloy in 1 M HCl medium. *J Mol Liq* 214:293–297

20. Kalaiselvi P, Chellammal S, Palanichamy S, Subramanian G (2010) *Artemisia pallens* as corrosion inhibitor for mild steel in HCl medium. *Mater Chem Phys* 120:643–648
21. Abdallah YM, Hassan HM, Shalabi K, Fouda AS (2014) Effects of *arctostaphylos uva-ursi* extract as green corrosion inhibitor for Cu<sub>10</sub>Ni alloy in 1 M HNO<sub>3</sub>. *Int J Electrochem Sci* 9:5073–5091
22. Shalabi K, Fouda AS, Elewady GY, El-Askalany A (2014) Adsorption and inhibitive properties of *Phoenix dactylifera* L. extract as a green inhibitor for Al and Al–silicon alloy in HCl. *Prot Met Phys Chem Surf* 50(3):420–431
23. Fouda AS, Tawfik H, Badr AH (2012) Corrosion inhibition of mild steel by *Camellia Sinensis* extract as green inhibitor. *Adv Mater Corros* 1:1–7
24. Shalabi K, Abdel NA (2015) Adsorption and inhibitive effect of *Schinus terebinthifolius* extract as a green corrosion inhibitor for carbon steel in acidic solution. *Pot Met Phys Chem Surf* 51(5):908–917
25. Fouda AS, Abdallah YM, Elawady GY, Ahmed RM (2015) Electrochemical study on the effectively of *Hyoscyamus Muticus* extract as a green inhibitor for corrosion of copper in 1 M HNO<sub>3</sub>. *J Mater Environ Sci* 5(6):1519–1531
26. Fouda AS, Mohamed AE, Khalid MA (2016) *Trigonella stellate* extract as corrosion inhibitor for copper in 1 M nitric acid solutions. *J Chem Pharm Res* 8(2):86–98
27. Rai N, Yadav S, Verma AK, Tiwari L, Sharma RK (2012) Monographic profile on quality specifications for a herbal drug and spice of commerce- CCE L. *Int J Adv Herb Sci Technol* 1:1–12
28. Al-Snafi AE (2016) the pharmacological activities of CCE. *IOSR J Pharm* 6:46–65
29. Fouda AS, Elabbasy HM (2019) Olive leaf as green corrosion inhibitor for C-steel in sulfamic acid solution. *Green Chem Lett Rev* 12:332–342
30. Iroha NB, Hamilton-Amachree A (2019) Inhibition and adsorption of oil extract of *Balanites aegyptiaca* seeds on the corrosion of mild steel in hydrochloric acid environment. *World Sci News* 126:183–197
31. Fouda AS, Rashwan SM, Darwish MMK, Arman NM (2018) Corrosion inhibition of Zn in a 0.5 M HCl solution by *Ailanthus altissima* extract. *Port Electrochim Acta* 36(4):309–323
32. Wang W, Shi W, Li CQ (2019) Time dependent reliability analysis for cast iron pipes subjected to pitting corrosion. *Int J Press Vessels Pip* 175:103935
33. Al-Itawi HI, Al-Mazaideh GM, Al-Rawajfeh AE, Al-Ma'abreh AM, Marashdeh A (2019) The effect of some green inhibitors on the corrosion rate of Cu, Fe and Al metals. *Int J Corros Scale Inhib* 8:199–211
34. Shalabi K, Abdallah YM, Fouda AS (2015) Corrosion inhibition of Al in 0.5 M HCl solutions containing phenyl sulfonylacetophenoneazo derivatives. *Res Chem Intermed* 41:4687–4711
35. Motawea MM, Gadow HS, Fouda AS (2016) Expired cidamex drug as corrosion inhibitor for Al in acidic solution. *Glob J Res Eng* 16(1):1–20
36. Shalabi K, Fouda AS, Elewady GY (2014) Adsorption and inhibitive properties of *Phoenix dactylifera* L. Extract as a green inhibitor for Al and Al–silicon alloy in HCl. *Prot Met Phys Chem Surf* 50:420–431
37. Jiang X-L, Lai C, Xiang Z, Yang Y-F, Tan B-L, Long Z-Q, Liu L-P, Yun-tian Gu, Yang W-J, Chen X (2018) Study on the extract of *Raphanus Sativus* L. as green corrosion inhibitor for Q235 steel in HCl solution. *Int J Electrochem Sci* 13:3224–3234
38. Eldesoky AM, Nozha SG (2017) The adsorption and corrosion inhibition of 8-hydroxy-7-quinolinecarboxaldehyde derivatives on C-steel surface in hydrochloric acid. *Chin J Chem Eng* 25:1256–1265
39. Velázquez-González MA, Gonzalez-Rodriguez JG, Valladares-Cisneros MG, Hermoso-Diaz IA (2014) Use of *Rosmarinus officinalis* as green corrosion inhibitor for carbon steel in acid medium. *Am J Anal Chem* 5:42143
40. Fouda AS, Eissa M, Fakh M (2019) Pomegranate aqueous extract (PAE) as an eco-friendly inhibitor for carbon steel used in sanitation plants: kinetics and bacteria effect. *J Bio Tribo Corros* 5:5
41. Fouda AS, Mohamed FS, El-Sherbeni MW (2016) Corrosion inhibition of Al–silicon alloy in hydrochloric acid solutions using carbamidic thioanhydride derivatives. *J Bio Tribo Corros* 2:11
42. Tripathy DB, Murmu M, Banerjee P, Quraishi MA (2019) Palmitic acid based environmentally benign corrosion inhibiting formulation useful during acid cleansing process in MSF desalination plants. *Desalination* 472:114128
43. Nathiya RS, Perumal S, Murugesan V, Raj V (2019) Evaluation of extracts of *Borassus flabellifer* dust as green inhibitors for Al corrosion in acidic media. *Mater Sci Semicond Process* 104:104674
44. Fouda AS, Zaki EG, Khalifa MMA (2019) Some new nonionic surfactants based on propane tricarboxylic acid as corrosion inhibitors for low carbon steel in hydrochloric acid solutions. *J Bio Tribo Corros* 5:31
45. Oguzie EE (2007) Corrosion inhibition of Al in acidic and alkaline media by *Sansevieria trifasciata* extracts. *Corros Sci* 49:1527–1539
46. Fouda AS, Abdel Nazeer A, El Behairy WT (2018) Assessment of begonia extract as new eco-friendly inhibitor for low-carbon-steel corrosion in acidic environment. *J. Bio Tribo Corros* 4:7
47. Fouda AS, Abdel Haleem E (2018) Berry leaves extract as green effective corrosion inhibitor for Cu in nitric acid solutions. *Surf Eng Appl Electrochem* 54:498–507
48. Fouda AS, El-Awady GY, El Behairy WT (2018) *Prosopis juliflora* plant extract as potential corrosion inhibitor for low-carbon steel in 1 M HCl solution. *J Bio Tribo Corros* 4:8
49. Hema K, Sirajunnisa AR, Venkatraman B (2015) the effect of solanam xanthocarpum leaves extract on corrosion inhibition of carbon steel in acidic medium. *Int J Adv Res Chem Sci (IJARCS)* 2:10–20
50. Fouda AS, El-Taweel FM, Mohamed NH (2020) Evaluation of the inhibition effect of some novel organic compounds (phenol derivatives) for corrosion of  $\alpha$ -brass in acid solutions. *Int J Electrochem Sci* 15:188–207
51. Fouda AS, Shalab K, Shaaban MS (2019) synergistic effect of potassium iodide on corrosion inhibition of carbon steel by *Achillea santolina* extract in hydrochloric acid solution. *J Bio Tribo Corros* 5:71
52. Onyeachu IB, Obot IB, Alamr AH (2020) Effective acid corrosion inhibitors for X60 steel under turbulent flow condition based on benzimidazoles: electrochemical, theoretical, SEM, ATR-IR and XPS investigations. *Eur Phys J* 135:129
53. Kavitha N, Kathiravan S, Jyoth S (2019) Adsorption and inhibitive properties of methanol extract of *Leucas aspera* leaves for the corrosion of mild steel in HCl medium. *J Bio Tribo Corros* 5:51
54. El-Azaly Ali M (2019) Influence of soybean (*Glycine Max*) plant extract on corrosion of Al in 1M HCl. *Int J Electrochem Sci* 14:2714–2731
55. Harb MB, Abubshait S, Etteyeb N, Kamoun M, Dhoub A (2020) Olive leaf extract as a green corrosion inhibitor of reinforced concrete contaminated with seawater. *Arab J Chem* 13:4846–4856
56. Elabbasy Hanaa M, Zidan Samir M, Fouda AS (2019) Inhibitive behavior of ambrosia maritima extract as aneco-friendly corrosion inhibitor for carbon steel in 1M HCl. *Zastita Materijala* 60:129–146
57. Radovanovic MB, Antonijevic MM (2016) Inhibition of brass corrosion by 2-mercapto-1-methylimidazole in weakly alkaline solution. *J Mater Eng Perform* 25:921–937
58. Fouda AS, Abdel Aal A, Abdel Haleem E (2017) *Calotropis Procera* extract (CPE) as corrosion inhibitor for copper in nitric acid

- medium. Bull Fac Sci Zagazig Univ. <https://doi.org/10.21608/bfszu.2017.31051>
59. Al-Nami SY, Fouda AE (2019) *Calotropis Procera* extract as corrosion inhibitor for copper in nitric acidic environment. Int J Electrochem Sci 14:6902–6919
  60. Yousefi A, Javadian S, Sharifi M (2019) An experimental and theoretical study of biodegradable gemini surfactants and surfactant/carbon nanotubes (CNTs) mixtures as new corrosion inhibitor. J Bio Tribo Corros 5:82
  61. Mahdavian M, Bagha AR, Alibakhshi E, Ashhari S, Palimi MJ, Farashi S, Javadian S, Ektefa F (2018) Corrosion of mild steel in hydrochloric acid solution in the presence of two cationic gemini surfactants with and without hydroxyl substituted spacers. Corros Sci 137:62–75
  62. Devi PN, Sathiyabama J, Rajendran S (2017) Study of surface morphology and inhibition efficiency of mild steel in simulated concrete pore solution by lactic acid–Zn<sup>2+</sup> system. Int J Corros Scale 6:18
  63. Kranthiraja K, Park H, Gunasekar K (2018) Impact of topology of alkoxy side chain in alkoxyphenylthiophene substituted benzodithiophene based 2D conjugated low bandgap polymers on photophysical and photovoltaic properties. Macromol Res 26:500–505
  64. Abdel-Fattah E, Alharthi AI, Fahmy T (2019) Spectroscopic, optical and thermal characterization of polyvinyl chloride-based plasma-functionalized MWCNTs composite thin films. Appl Phys 125:475
  65. Woo JC, Kim SG, Koo JG, Kim GH, Kim DP, Yu CH, Kang JY, Kim CI (2009) A study on dry etching for profile and selectivity of ZrO<sub>2</sub> thin films over Si by using high density plasma. Thin Solid Films 517:4246–4250

**Publisher's Note** Springer Nature remains neutral with regard to jurisdictional claims in published maps and institutional affiliations.